Supplementary information

Ethanol combustion assisted fast synthesis of tri-metal oxides with reduced graphene oxide for outperformed overall water splitting performance

Zehua Zou [a], Zhenan Zheng [a], Yingyu Chen [a], Yong Shao [c], Xuan Zheng [a], Chuan Zhao,*[b] and Qingxiang Wang *[a]

[a] Fujian Provincial Key Laboratory of Modern Analytical Science and Separation Technology, College of Chemistry, Chemical Engineering and Environment, Minnan Normal University, Zhangzhou 363000, China

[b] School of Chemistry and Materials & Manufacturing Futures Institute, University of New South Wales, Sydney 2052, Australia

[c] Key Laboratory of the Ministry of Education for Advanced Catalysis Materials, College of Chemistry and Materials Science, Zhejiang Normal University, Jinhua 321004, China

*Corresponding author: chuan.zhao@unsw.edu.au

axiang236@vip.163.com

Experimental section

1. Chemicals

Iron (III) nitrate nonahydrate ($Fe(NO_3)_3·9H_2O$, Xilong Chemical), nickel (II) chloride hexahydrate ($NiCl_2·6H_2O$, Xilong Scientific), cobalt (II) chloride hexahydrate ($CoCl_2·6H_2O$, Aladdin Reagent), potassium hydroxide (KOH, Xilong Chemical), hydrochloric acid (HCl, Xilong Scientific), ethanol (C_2H_5OH, Xilong Chemical), nickel foam (NF, Changsha Liyuan), iridium oxide (IrO_2, Aladdin Reagent), platinum-carbon (10 wt% Pt/C, Aladdin Reagent) and perfluorinated resin solution (5% Nafion, Sigma Aldrich). All reagents used in the experiments were used as received, and the experimental solutions were prepared with deionized water.

2. Preparation of catalysts on NF by SCS

Prior to preparation, a piece of NF (1 cm × 1 cm) was cleaned with 3 M HCl aqueous solution, ethanol and deionized water for 10 min by ultrasonication, respectively. Then, 0.40 g (1 mmol) of $Fe(NO_3)_3·9H_2O$, 0.24 g (1 mmol) of $NiCl_2·6H_2O$ and 0.24 g (1 mmol) of $CoCl_2·6H_2O$ were weighed into a porcelain crucible. Followed by, 6 mL of ethanol was added and stirred to form a homogeneous solution. Thereafter, the pretreated NF was soaked in the above trimetallic mixture solution for 10 min to be fully impregnated, and then the solution was ignited by lighter to make it burn completely. The burnt NF was washed with ethanol and deionized water for several times, and dried at 60 ℃ for overnight in vacuum, to obtain the final product of FeCoNiOx-rGO/NF electrode. The loading of FeCoNiOx-rGO on FeCoNiOx-rGO/NF electrode was about 52 mg, determined by weighing the difference before and after combustion.

For comparison, the control electrodes of monometallic FeOx-rGO/NF, CoOx-rGO/NF and NiOx-rGO/NF electrodes were obtained by the same synthetic method, expect replacing the trimetallic mixture with the single $Fe(NO_3)_3·9H_2O$, $NiCl_2·6H_2O$ or $CoCl_2·6H_2O$ ethanol solution. The rGO-NF electrode was obtained by the same process without adding any metal salt.

The benchmark catalysts (IrO_2 or Pt-C) modified electrodes were obtained by drop coating. The ink was composed of 0.2 mL of ethanol, 0.8 mL of deionized water, 40

μL of 5% Nafion solution and 4 mg of IrO_2 or Pt-C powders. Then the ink was dropped onto the treated NF and dried overnight to obtain the final IrO_2/NF or Pt-C/NF electrodes.

3. Physical characterization

X-ray diffraction (XRD) was performed on a Germany Bruker D8 Advance-X diffractometer. Fourier transform infrared (FT-IR) was obtained on a USA Thermo Fisher Scientific NICOLET iS 10 spectrometer. Raman was performed on a French Horiba Jobin Yvon JYHR900 spectrometer. Scanning electron microscope (SEM) was carried on a Japanese Hitachi S-4800 instrument. Energy dispersive X-ray spectroscopy (EDX) element mapping images were obtained by TESCAN MIRA LMS SEM instrument. Transmission electron microscope (TEM) and high-resolution TEM (HRTEM) were carried out on USA FEI Tecnai G20 instrument. X-ray photoelectron spectroscopy (XPS) was performed on a USA Thermo Fisher Scientific Kratos Axis Ultra instrument with C1s binding energy (284.80 eV) as the energy standard.

4. Electrochemical measurements

Chenhua CHI 660E electrochemical station (China) was used to test the electrochemical performance by using the standard three-electrode system in 1.0 M KOH electrolyte. The NF (1×1 cm^2) loading with electrocatalysts was used as the working electrode, and Hg/HgO (1.0 M KOH) as the reference electrode, and the carbon rod as the counter electrode. The sweep rate of all linear sweep voltammetry (LSV) polarization curves was 5 mV s^{-1}. The Tafel slope was calculated by plotting the overpotential (η) *vs.* logarithm of current density (log j) using the LSV polarization curves. The electrochemical impedance spectroscopy (EIS) test in OER and HER process were set as 0.55 V and -1.05 V, respectively (*vs.* Hg/HgO) with a frequency range from 10 kHz to 0.01 Hz and an amplitude of 5 mV. The equivalent circuit diagram was employed to fit the EIS curves for the analysis of charge transfer resistance (R_{ct}) as follows:

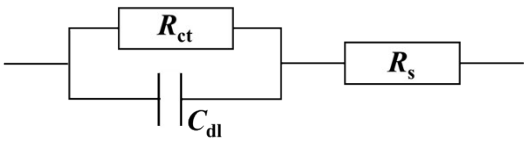

Besides, 85% iR compensation was applied to all the LSV curves to enhance the repeatability of experimental data, where the R-value of each electrocatalyst was manually obtained as the solution resistance (R_s) from EIS curves.

Electrochemical active surface area (ECSA) was determined by measuring the double layer capacitance (C_{dl}) current in the non-Faraday range (0~ 0.1 V vs. Hg/HgO). Scan rates were performed at 30, 50, 70, 90 and 110 mV s^{-1}, respectively. The C_{dl} values were converted into ECSA using the specific capacitance as a standard for the same system. In this context, C_{dl} values were directly utilized to normalize the measured current density of LSV curves. The stability measurements were investigated by potential-time curve (*p-t*) and cyclic voltammetry (CV) test with a scanning rate of 50 mV s^{-1}. The conversion of measured potential to the reversible hydrogen electrode potential (RHE) is calculated by the following equation: $E_{vs.RHE} = E_{vs.Hg/HgO} + 0.098 + 0.059pH$. The two-electrode system assembled with FeCoNiOx-rGO/NF as both anode and cathode was used to investigate the overall water splitting performance of the electrocatalysts.

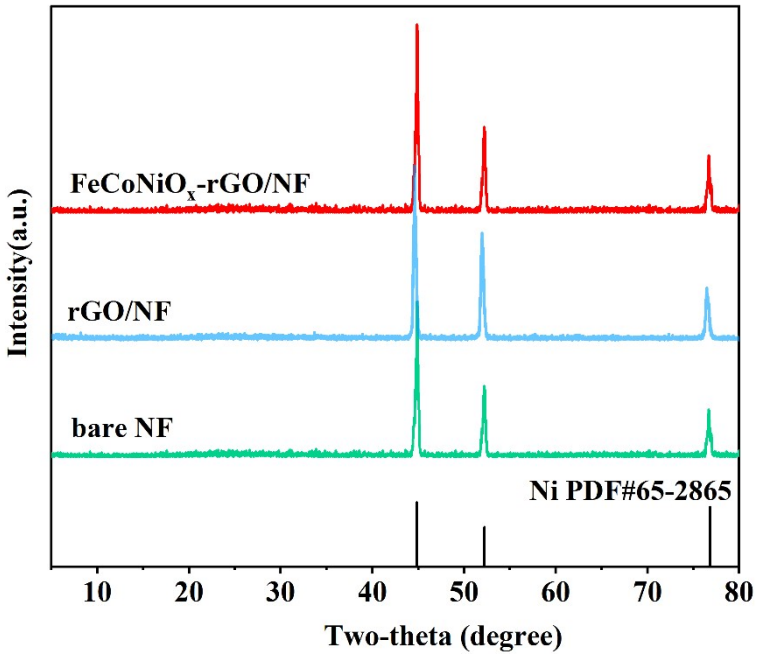

Fig. S1. XRD patterns of FeCoNiOx-rGO/NF and rGO/NF.

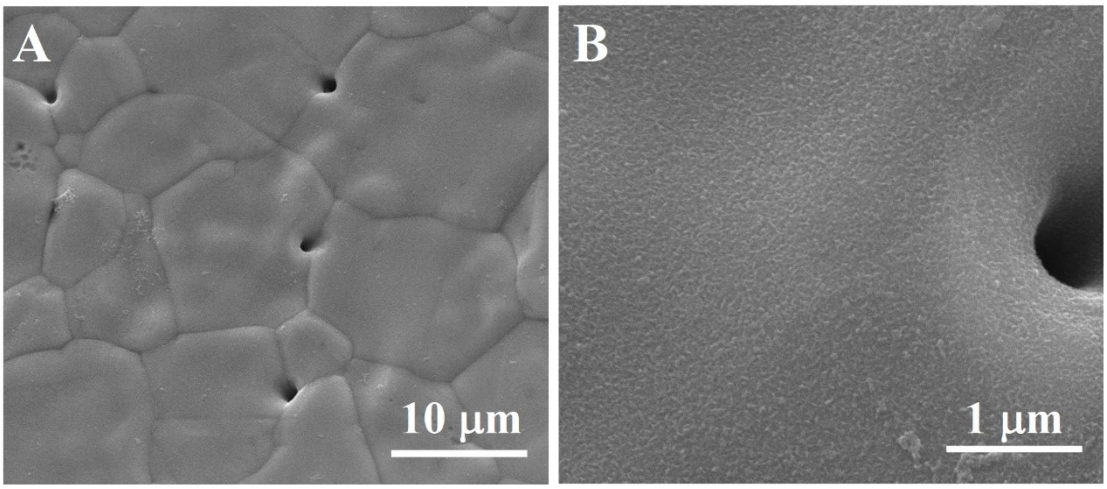

Fig. S2. SEM images of NF with different magnification.

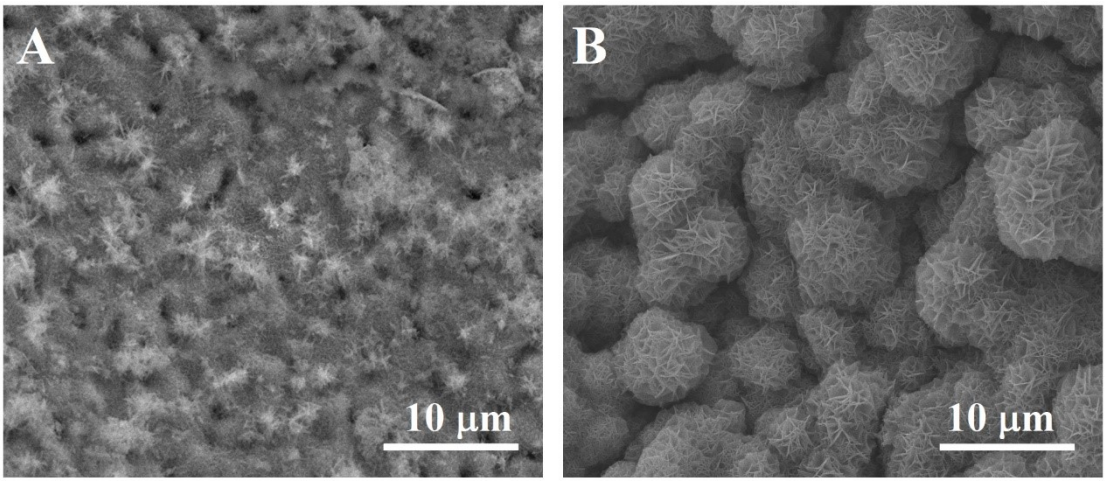

Fig. S3. SEM images of (A) rGO/NF and (B) FeCoNiOx-rGO/NF at low magnification.

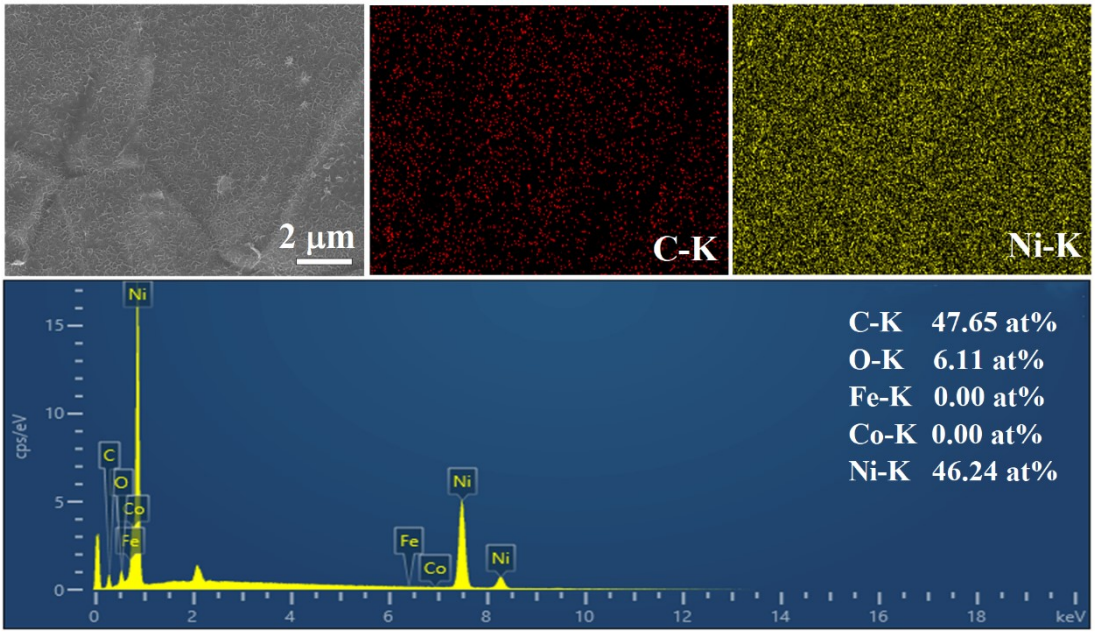

Fig. S4. The EDX element mapping images of rGO/NF.

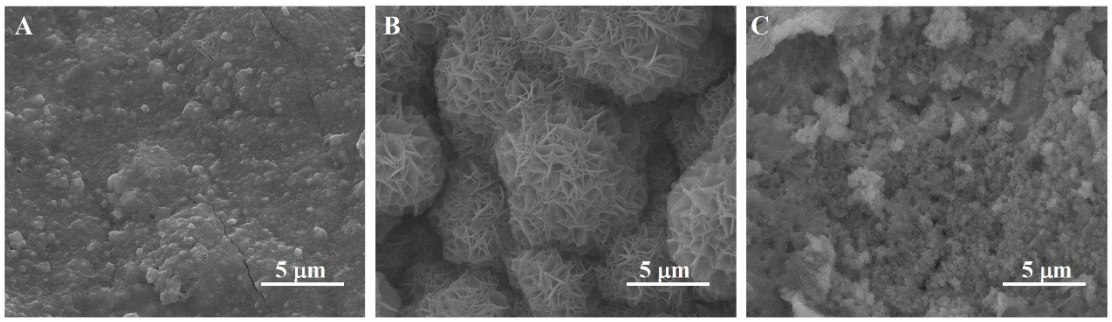

Fig. S5. SEM images of FeCoNiOx-rGO/NF electrodes with the adding quantity of metal salts of (A) 0.2 mmol, (B) 1 mmol and (C) 2 mmol.

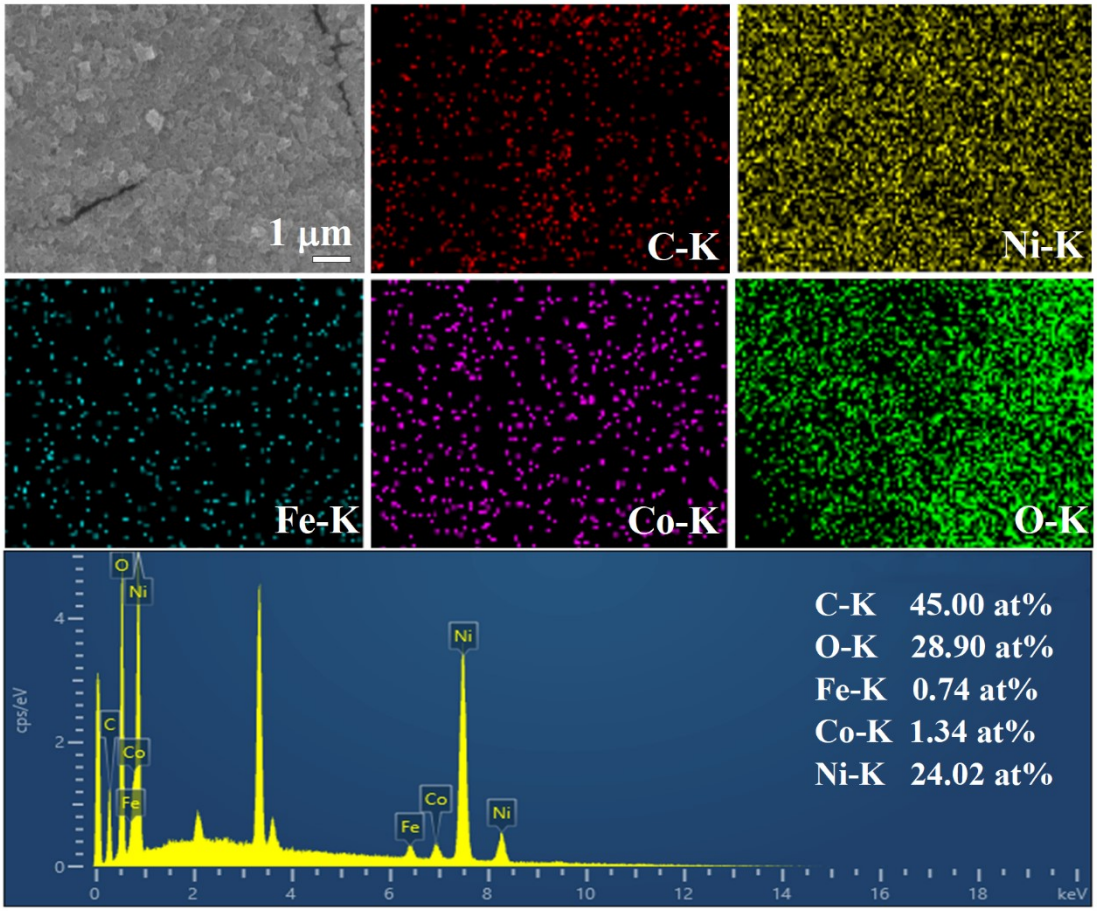

Fig. S6. The EDX element mapping images of FeCoNiOx-rGO/NF.

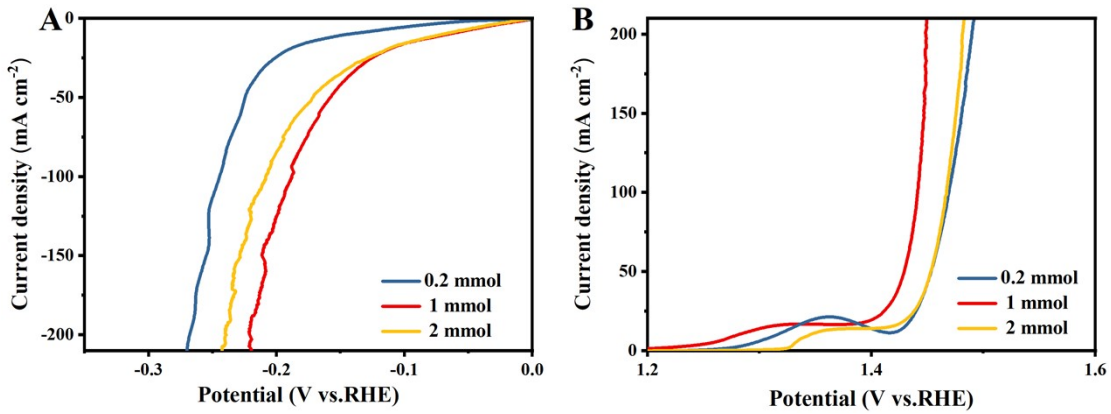

Fig. S7. (A) HER and (B) OER LSV curves of FeCoNiOx-rGO/NF with different raw material feeding.

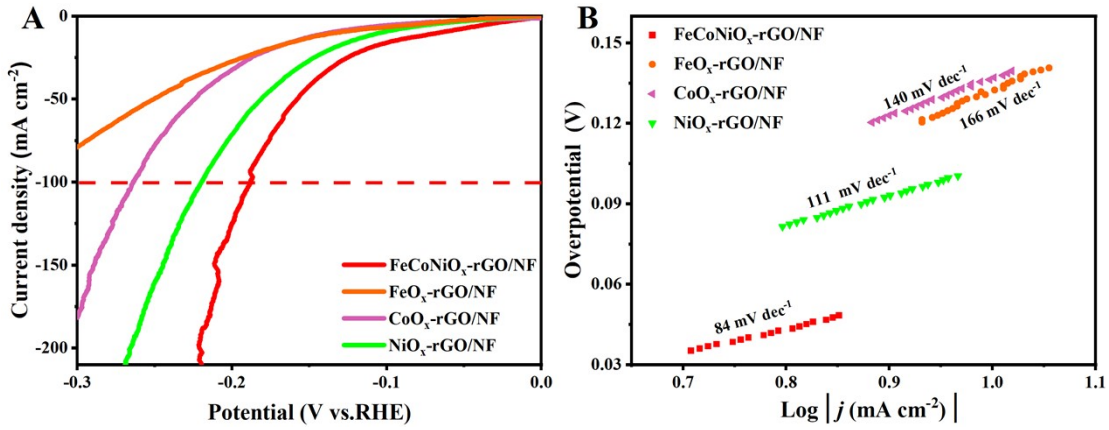

Fig. S8. (A) HER LSV curves and (B) Tafel curves of FeCoNiOx-rGO/NF, FeOx-rGO/NF, CoOx-rGO/NF and NiOx-rGO/NF.

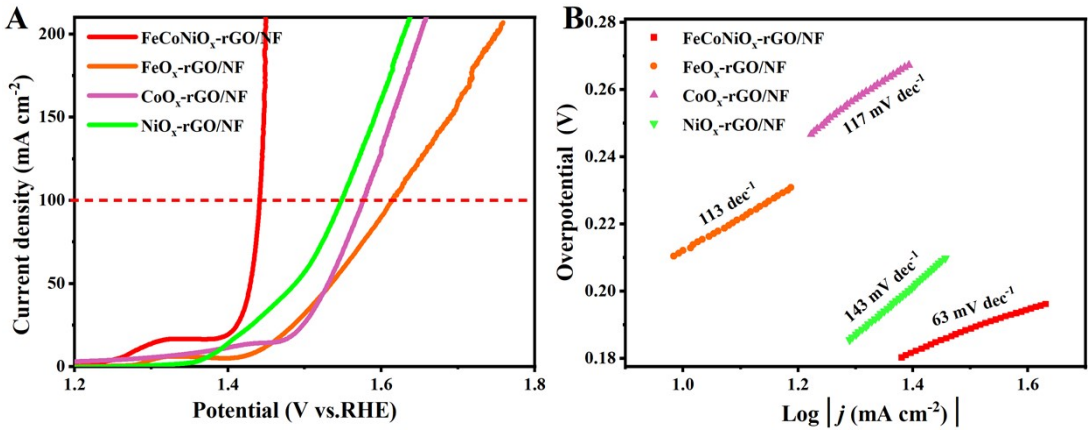

Fig. S9. (A) OER LSV curves and (B) Tafel curves of FeCoNiOx-rGO/NF, FeOx-rGO/NF, CoOx-rGO/NF and NiOx-rGO/NF.

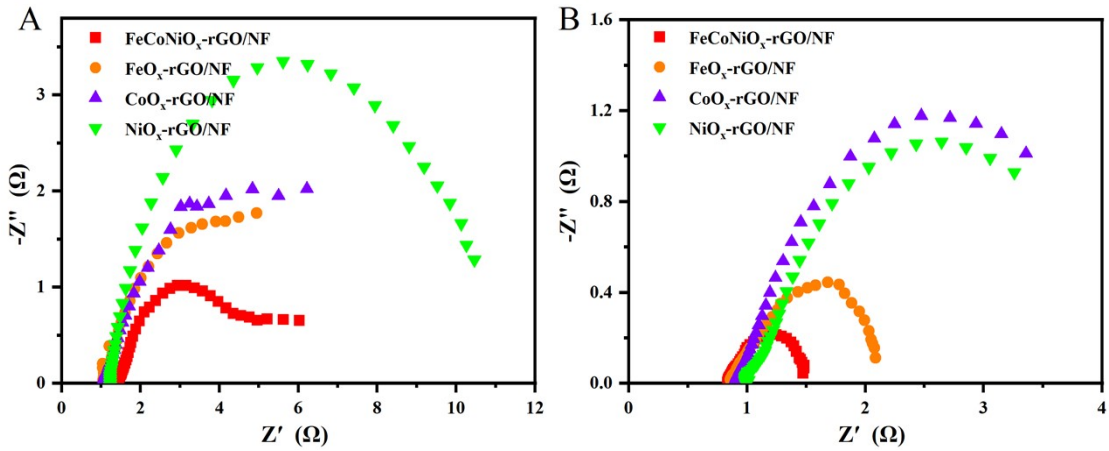

Fig. S10. EIS curves of FeCoNiOx-rGO/NF, FeOx-rGO/NF, CoOx-rGO/NF and NiOx-rGO/NF for (A) HER and (B) OER, respectively.

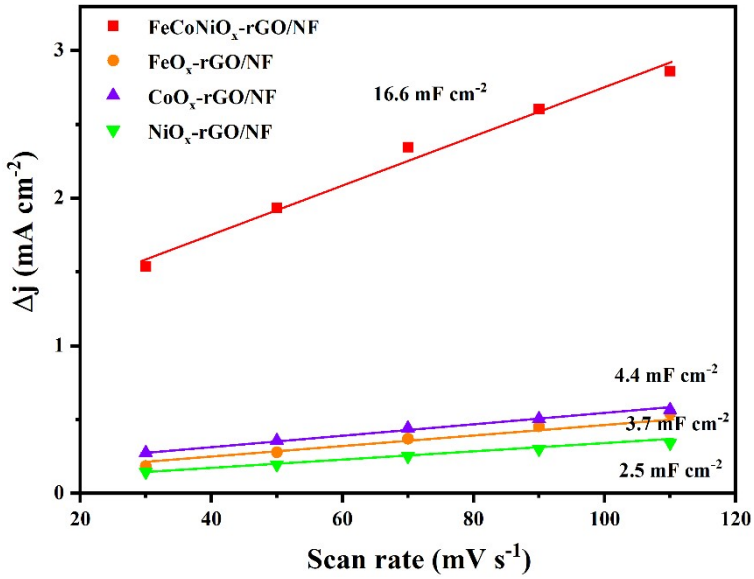

Fig. S11. C_{dl} curves of FeCoNiOx-rGO/NF, FeOx-rGO/NF, CoOx-rGO/NF and NiOx-rGO/NF, respectively.

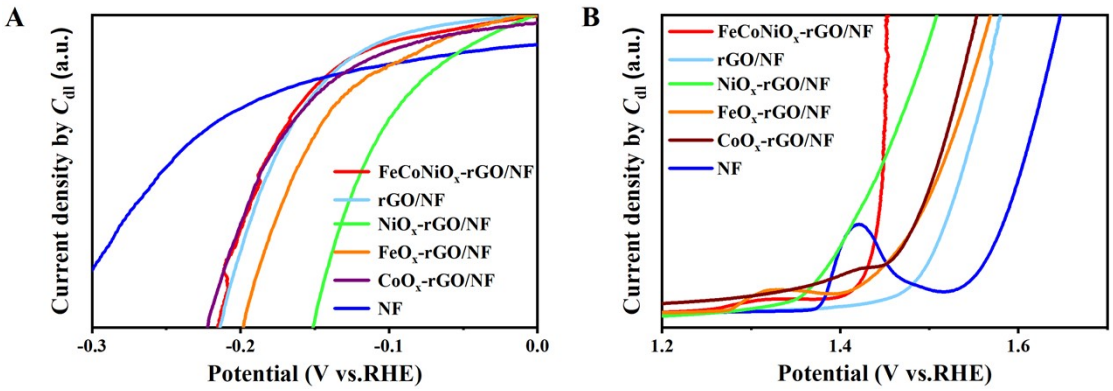

Fig. S12. (A) HER and (B) OER LSV curves normalized by C_{dl}-values of FeCoNiOx-rGO/NF, rGO/NF, FeOx-rGO/NF, CoOx-rGO/NF, NiOx-rGO/NF and NF, respectively.

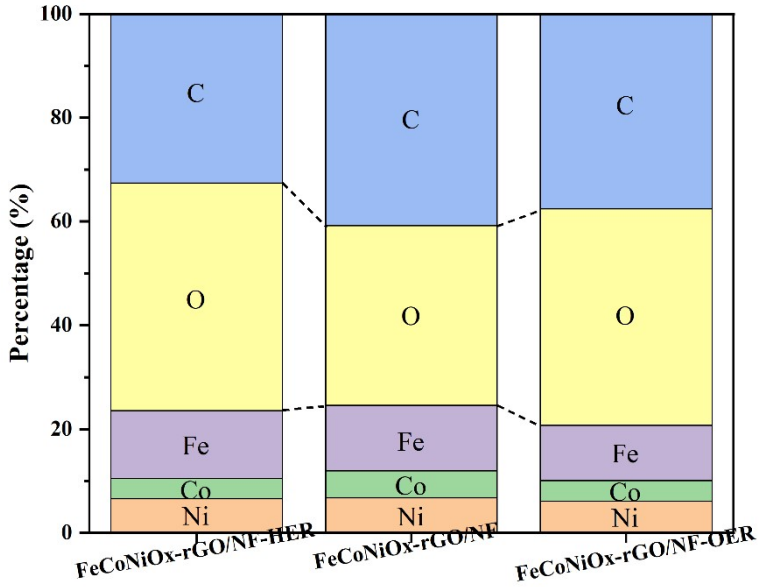

Fig. S13. The atomic percentage of C, O, Fe, Co and Ni of FeCoNiOx-rGO/NF, FeCoNiOx-rGO/NF-HER and FeCoNiOx-rGO/NF-OER from the XPS results.

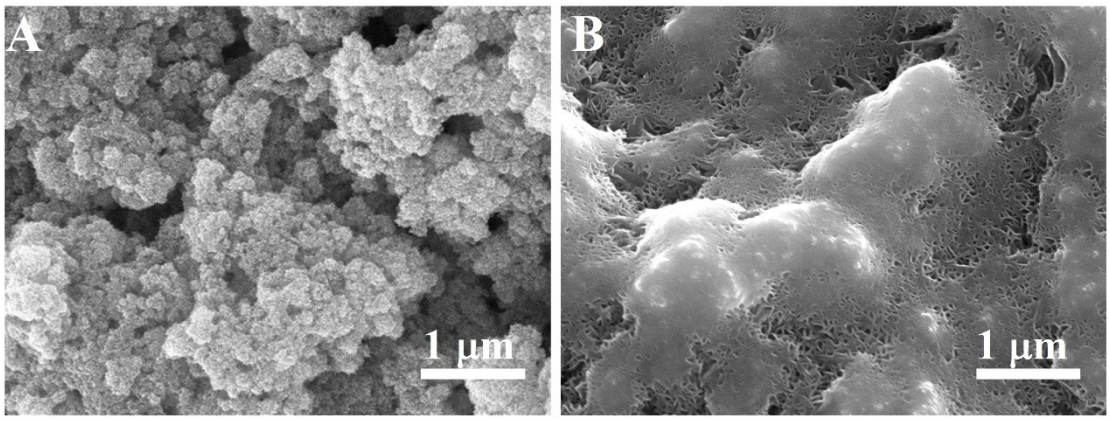

Fig. S14. SEM images of (A) FeCoNiOx-rGO/NF-HER and (B) FeCoNiOx-rGO/NF-OER.

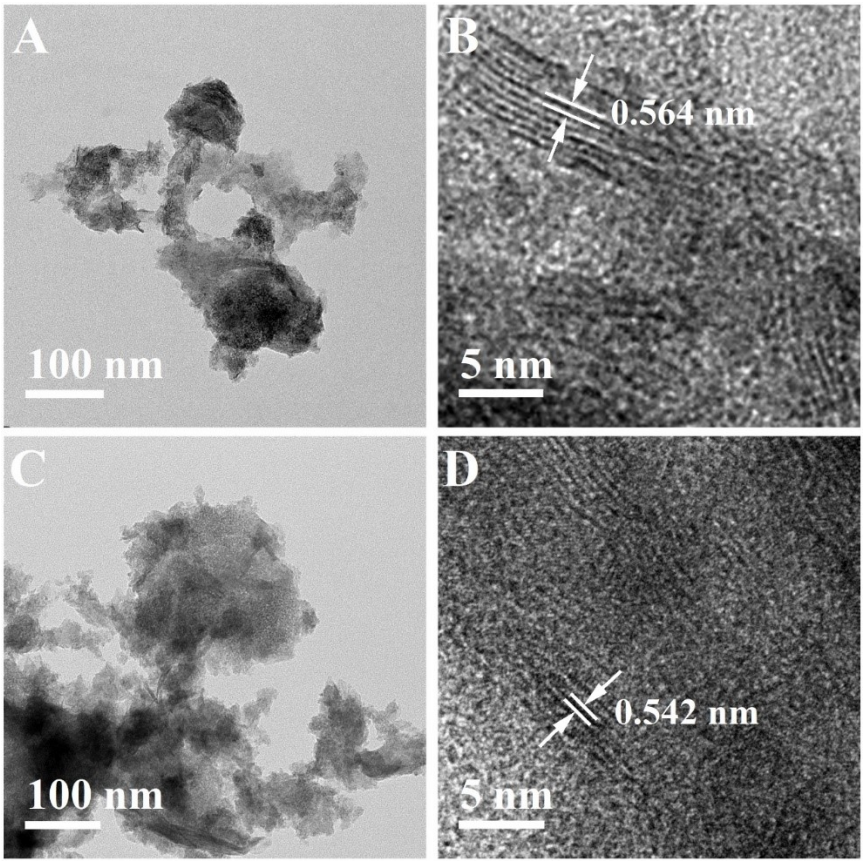

Fig. S15. TEM and HRTEM images of (A, B) FeCoNiOx-rGO/NF-HER and (C, D) FeCoNiOx-rGO/NF-OER.

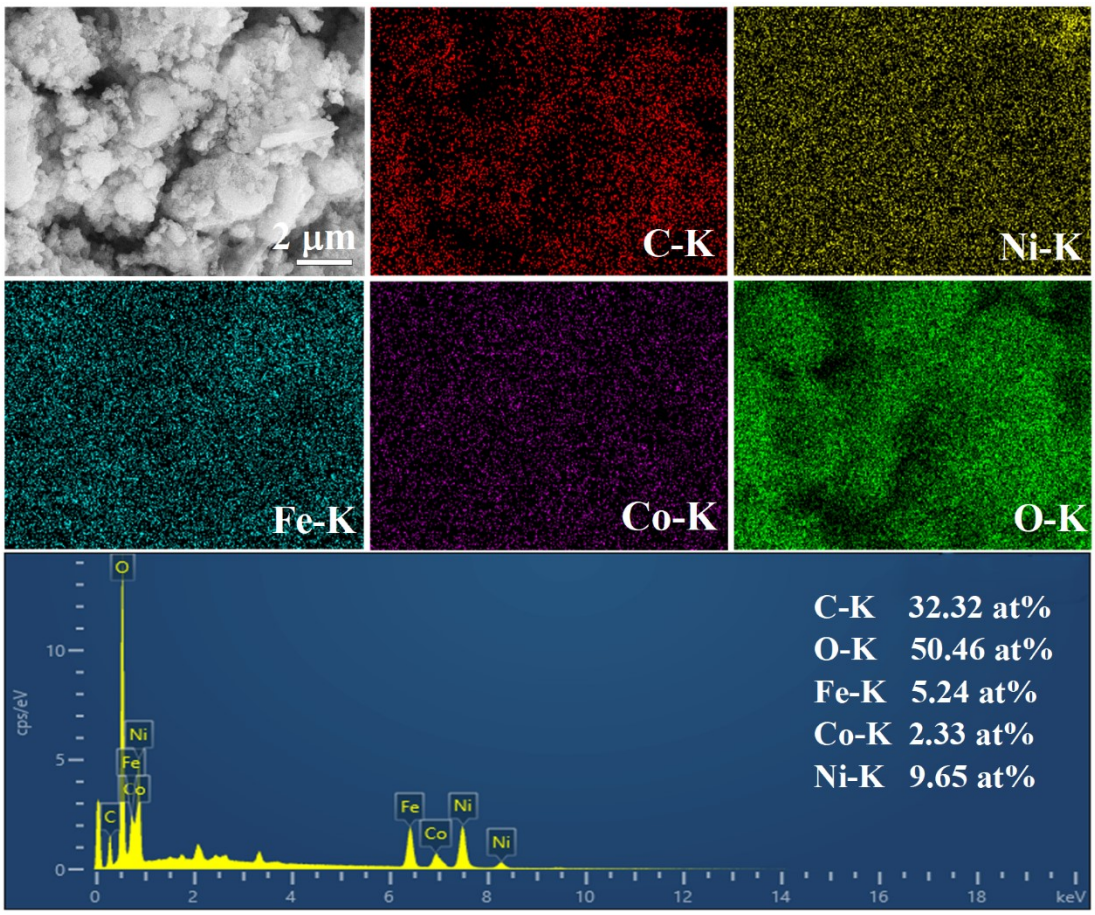

Fig. S16. The EDX element mapping images of FeCoNiOx-rGO/NF-HER.

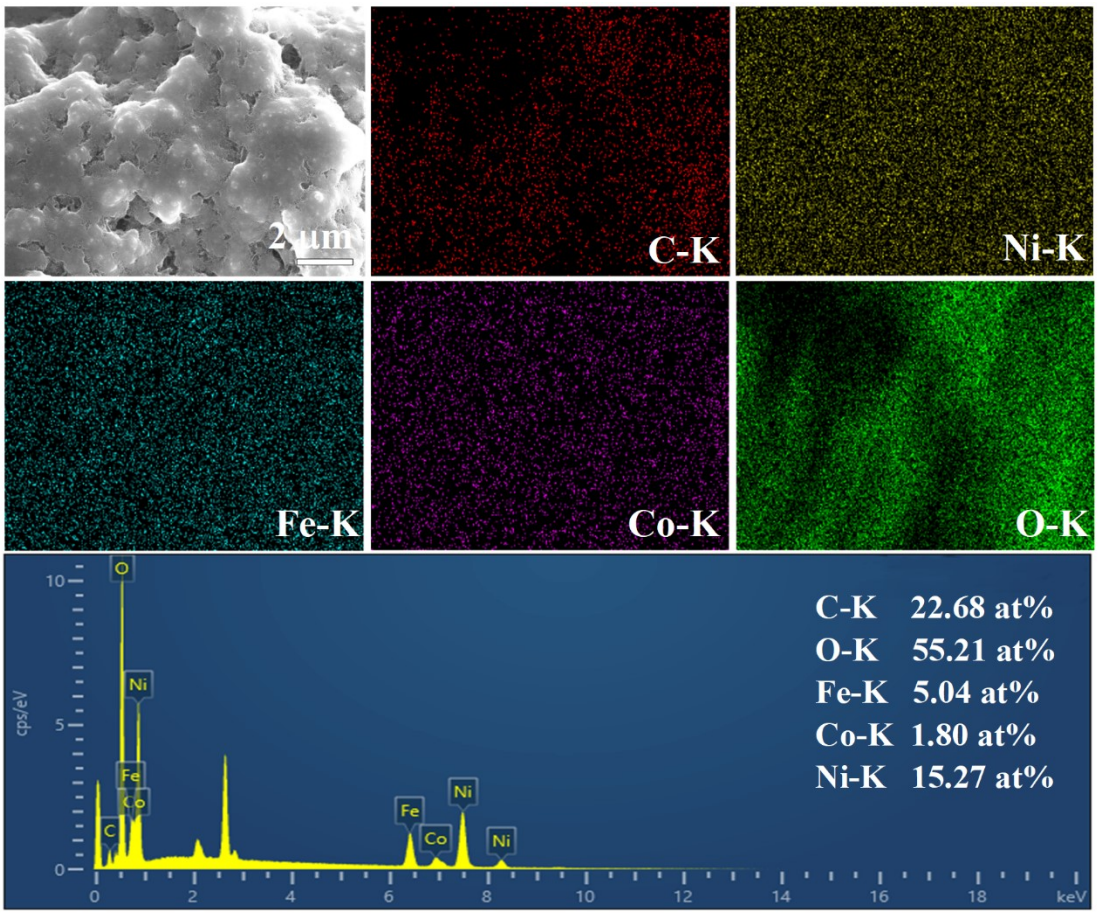

Fig. S17. The EDX element mapping images of FeCoNiOx-rGO/NF-OER.

Table S1. Comparison of this work and other recent bifunctional electrocatalysts at a test current density of 100 mA cm^{-2}.

Electrode couples	Cell voltage/V	Duration/h	Ref.
MNF-2	1.82	100	[1]
Mn_2P-Mn_2O_3/PNCF	1.70	72	[2]
CuNi@NiSe	~1.85	25	[3]
Ni-Co-Fe-P NBs	~1.58	100	[4]
S-FeNi/NF	1.81	200	[5]
NiFeCuP	~1.87	20	[6]
MnCoP/NF	1.97	240	[7]
Fe_2P-Co_2P/NF	1.64	100	[8]
FeCoNiOx-rGO/NF	**1.83**	**170**	**This work**

a: manual measured from the figures

References

[1] N. S. Gultom, T.-S. Chen, M. Z. Silitonga and D.-H. Kuo, Overall water splitting realized by overall sputtering thin-film technology for a bifunctional MoNiFe electrode: A green technology for green hydrogen, *Appl. Catal. B-Environ.*, 2023, **322**, 122103.

[2] X. Wang, G. Huang, Z. Pan, S. Kang, S. Ma, P. K. Shen and J. Zhu, One-pot synthesis of Mn_2P-Mn_2O_3 heterogeneous nanoparticles in a P, N-doped three-dimensional porous carbon framework as a highly efficient bifunctional electrocatalyst for overall water splitting, *Chem. Eng. J.*, 2022, **428**, 131190

[3] D. Gao, J. Shao, Y. Cui, L. Zhang and D. Cheng, Interfacial engineering of copper–

nickel selenide nanodendrites for enhanced overall water splitting in alkali condition, *Small*, 2023, **19**, 2301613.

[4] A. Li, L. Zhang, F. Wang, L. Zhang, L. Li, H. Chen and Z. Wei, Rational design of porous Ni-Co-Fe ternary metal phosphides nanobricks as bifunctional electrocatalysts for efficient overall water splitting, *Appl. Catal. B-Environ.*, 2022, **310**, 121353.

[5] K. Feng, R. Song, J. Xu, Y. Chen, C. Lu, Y. Li, W. Hofer, H. Lin, Z. Kang and J. Zhong, The S-Fe(Ni) sub-surface active sites for efficient and stable overall water splitting, *Appl. Catal. B-Environ.*, 2023, **325**, 122365.

[6] J. Ge, S. Diao, J. Jin, Y. Wang, X. Zhao, F. Zhang and X. Lei, NiFeCu phosphides with surface reconstruction via the topotactic transformation of layered double hydroxides for overall water splitting, *Inorg. Chem. Front.*, 2023, **10**, 3515-3524

[7] W.-Y. Fu, Y.-X. Lin, M.-S. Wang, S. Si, L. Wei, X.-S. Zhao and Y.-S. Wei, Sepaktakraw-like catalyst Mn-doped CoP enabling ultrastable electrocatalytic oxygen evolution at 100 mAcm22 in alkali media, *Rare Met.*, 2022, **41**, 3069-3077.

[8] H. Zhang, H. Li, Y. Zhou, F. Tan, R. Dai, X. Liu, G. Hu, L. Jiang, A. Chen and R. Wu, Heterostructured bimetallic phosphide nanowire arrays with lattice-torsion interfaces for efficient overall water splitting, *J. Energy Chem.*, 2023, **77**, 420-427.